

Single-Image Optical Center Estimation from Vignetting and Tangential Gradient Symmetry

Yuanjie Zheng¹ Chandra Kambhamettu¹ Stephen Lin²

zheng.vision@gmail.com chandra@cis.udel.edu stevelin@microsoft.com

¹Video/Image Modeling and Synthesis (VIMS) Lab.

Department of Computer Science, University of Delaware, Newark, DE, USA

²Microsoft Research Asia, Beijing, P.R. China

Abstract

In this paper, we propose a method for estimating the optical center of a camera given only a single image with vignetting. This is accomplished by identifying the center of the vignetting effect in the image through an analysis of semicircular tangential gradients (SCTGs). For a given image pixel, the SCTG is the image gradient along the tangential direction of the circle centered at the currently estimated optical center and passing through the pixel. We show that for natural images with vignetting, the distribution of SCTGs is generally symmetric if the optical center is estimated accurately, but is skewed otherwise. By minimizing the asymmetry of the SCTG distribution with nonlinear optimization, our method is able to obtain reliable estimates of the optical center. Experiments on simulated and real vignetting images demonstrate the effectiveness of this technique.

1. Introduction

In a digital camera, the point at which the optical axis intersects the sensor plane is commonly referred to as the optical center, image center, or principal point. Knowledge of a camera's optical center is required in modeling many imaging properties [18] such as vignetting, radial lens distortion, and field curvature. These properties are often characterized as being radially symmetric about the optical center, as they generally result from the circular construction of lens components. In addition, accurate determination of the optical center is needed in many geometry-based computer vision applications, including 3D vision [5], shape from shading, and geometric reasoning [11].

Camera manufacturers seldom provide data on the optical center of a camera. Moreover, manufacturing generally tolerates significant variations in the position of the optical

center with respect to imaging parameters such as focus and zoom [18]. As a result, the user is left to estimate the different optical centers for different camera parameters.

Various techniques have been proposed for optical center estimation. Some works simply assume the optical center to be at the numerical center of the image coordinates [19, 20]. However, in practice the numerical center may differ from the true optical center by as many as 30-40 pixels [5]. Other methods estimate the optical center by locating the center of an optical effect such as vignetting [8], radial lens distortion [17], vanishing point [15], or focus/defocus [18]. These techniques generally require specific calibration scenes or instruments, such as a uniform scene [8], a special calibration target [17], a cube [15], a high-frequency textured pattern [18], or a laser emitter [5]. A third approach to estimate the optical center is to use a general camera calibration procedure that also estimates other intrinsic or extrinsic camera parameters. Some of these methods require a particular calibration pattern or scene [14, 4], while others perform self-calibration using image sequences captured with fixed camera settings [1, 3].

In this paper, we show that it is possible to solve an important task that is particularly difficult for previous methods: estimating the optical center from a single image of an arbitrary natural scene. We propose an approach that does not require strict scene conditions, special calibration patterns, image sequences, or even the camera to be in hand. This makes the method convenient in practice, especially when processing a single image captured with an unknown camera and lens, as is typically the case for photographs taken from the web.

The proposed approach can work when the image contains vignetting. It utilizes basic properties of vignetting, namely radial symmetry and increasing light attenuation towards the image boundaries, to locate the optical center. To perform this task reliably for an image of an arbitrary nat-

ural scene, our method examines distributions of semicircular tangential gradients (SCTG). The SCTG at a pixel is defined as the gradient along the tangential direction of the circle that is centered at the currently estimated optical center and passes through the pixel. We show that the SCTG distribution for a broad range of vignetted images is symmetric for a correctly estimated optical center, but is skewed if the estimation is erroneous. We describe an efficient technique to estimate the optical center based on minimizing the asymmetry of the SCTG distribution using nonlinear optimization. The effectiveness of our technique is supported by experiments on both simulated and real vignetting images, and in the application of vignetting correction.

2. Semicircular Tangential Gradients

The gradient distributions of natural images have been shown to share certain characteristics such as zero-mean symmetry and a heavy-tailed form. These properties have recently been used to reach higher levels of performance in a number of different computer vision applications, including image denoising, deblurring, inpainting, superresolution, and vignetting correction [21, 2, 13, 7, 6, 10, 16, 20]. A brief review of these approaches can be found in [20].

In this paper, we study the distribution of a particular type of gradient, namely the semicircular tangential gradient. Our observation is that for a large range of natural images, the distribution of SCTGs is symmetric if the image is vignetting-free or if it contains vignetting with a correctly estimated optical center. Otherwise, for a vignetted image with an erroneously estimated optical center, the distribution is skewed.

2.1. SCTG Definition

Let Z denote a given image with vignetting. To index a pixel in Z , we will interchangeably use Euclidean coordinates and polar coordinates for simplicity in exposition. When using polar coordinates, we take the true optical center to be the origin of the coordinate system.

The conventional tangential gradient (TG) of a pixel (x, y) is the image gradient along the tangential direction of the circle that is centered at the true optical center (x_0, y_0) and passes through the pixel. In the polar coordinate system, the TG magnitude of a pixel (r, θ) can be expressed as

$$\psi_t^Z(r, \theta) = \frac{\partial Z(r, \theta)}{\partial \theta}. \quad (1)$$

We now define two semicircular TGs to be used in the estimation of the optical center. Here, we denote the estimate of the optical center as (x'_0, y'_0) . For a pixel (x', y') , the unit vector of its radial direction with respect to (x'_0, y'_0)

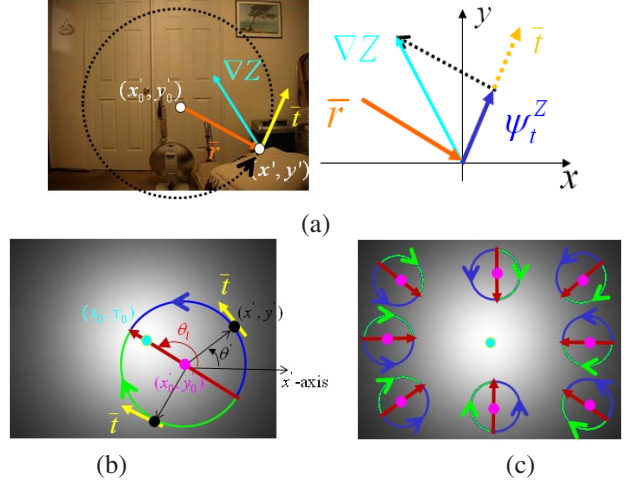


Figure 1. Illustration of semicircular tangential gradients (SCTG). (a) Counterclockwise SCTG. (b) Assignment of clockwise or counterclockwise SCTGs. (c) Effect of estimated optical center on SCTG assignment using Eq. (6), where the pink dots are different optical center estimates and the light blue dot is the true optical center.

is defined as

$$\bar{r}(x', y') = \begin{cases} \frac{[x' - x'_0, y' - y'_0]^T}{|[x' - x'_0, y' - y'_0]^T|} & |[x' - x'_0, y' - y'_0]^T| > 0 \\ [0, 0]^T & |[x' - x'_0, y' - y'_0]^T| = 0 \end{cases} \quad (2)$$

The direction of the *clockwise* or *counterclockwise* SCTG is obtained by rotating $\bar{r}(x', y')$ by 90° clockwise or counterclockwise, respectively, as expressed by

$$\bar{t}(x', y') = \text{sgn}(x', y') \begin{bmatrix} 0 & -1 \\ 1 & 0 \end{bmatrix} \bar{r}(x', y') \quad (3)$$

for which we set $\text{sgn}(x', y') = -1$ for the clockwise tangential direction, and $\text{sgn}(x', y') = 1$ for the counterclockwise case.

We define the clockwise SCTG and counterclockwise SCTG for a pixel as the image gradients along its clockwise tangential direction and counterclockwise tangential direction respectively. With the conventional image gradient operator $\nabla Z(x', y')$ defined in the Euclidean coordinate system as

$$\nabla Z(x', y') = \left[\frac{\partial Z(x', y')}{\partial x'}, \frac{\partial Z(x', y')}{\partial y'} \right]^T, \quad (4)$$

the magnitude of the clockwise or counterclockwise SCTG can be computed by

$$\psi_t^Z(x', y') = \nabla Z(x', y') \cdot \bar{t}(x', y'), \quad (5)$$

as shown in Fig. 1(a) for the counterclockwise case. From this definition, it can be seen that when $(x'_0, y'_0) = (x_0, y_0)$ the counterclockwise SCTG is equivalent to the conventional TG in Eq. (1).

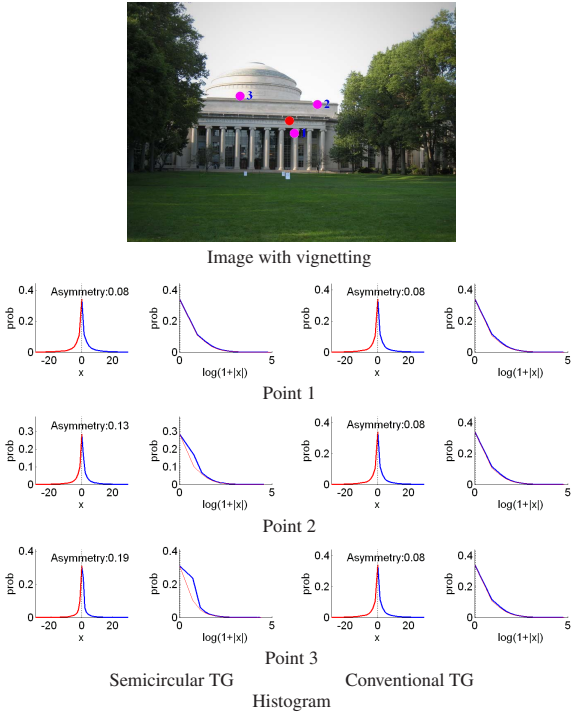


Figure 2. Comparison of semicircular tangential gradient (SCTG) and conventional TG distributions. The true optical center and three estimated optical centers are marked by the red dot and three purple dots, respectively. With each distribution, a $\log(1 + |x|)$ histogram is also shown to emphasize asymmetry.

In our method for estimating the optical center, we assign to each pixel either its clockwise SCTG or its counterclockwise SCTG according to its position with respect to the line defined by (x'_0, y'_0) and (x_0, y_0) , shown in red in Fig. 1(b). This line divides circles centered at (x'_0, y'_0) into two parts, shown in green and blue. Those pixels that lie on the green semicircle take the value of the clockwise SCTG, while those in blue use the counterclockwise TG. Equivalently, the image may be divided by the line through (x'_0, y'_0) and (x_0, y_0) , with clockwise SCTG values assigned to pixels on one side and counterclockwise SCTGs for the other.

This assignment of a clockwise or counterclockwise SCTG value to a pixel such as (x', y') in Fig. 1(b) can be expressed analytically by setting $\text{sgn}(x', y')$ in Eq. (3) according to Eq. (6), where θ_l denotes the rotation angle from the x' direction to the ray from (x'_0, y'_0) to (x_0, y_0) and is set to zero when $(x'_0, y'_0) = (x_0, y_0)$, and θ' is the polar angle of (x', y') with respect to (x'_0, y'_0) . With the SCTG value of each pixel determined according to Eqs. (2)-(6), pixels may be assigned in different ways depending on the estimate of the optical center, as shown for different estimates in Fig. 1(c).

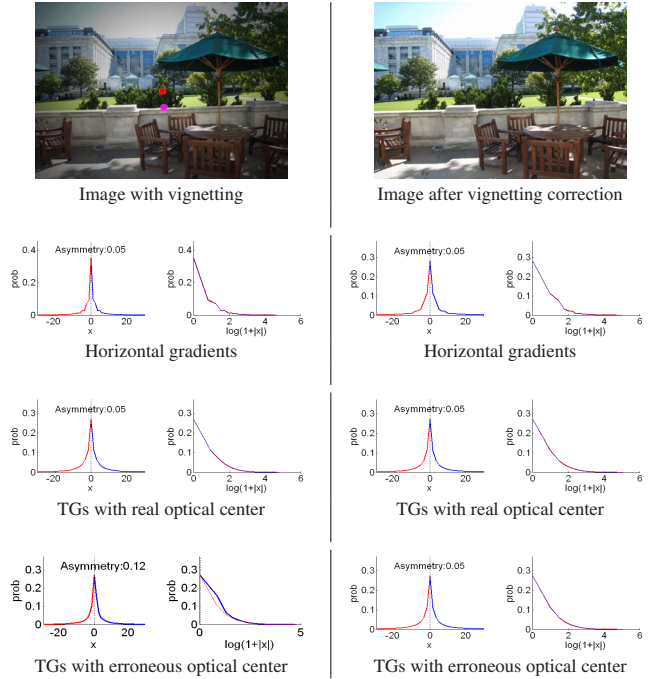


Figure 3. Comparison of semicircular tangential gradient (SCTG) and horizontal gradient distributions. In each image, the true optical center and estimated optical center are marked by the red dot and purple dot, respectively. With each distribution, a $\log(1 + |x|)$ histogram is also shown to emphasize asymmetry.

2.2. SCTG Distributions

In this section, we first present the useful distribution properties of SCTGs for images with vignetting. Then, we provide a geometric analysis on why vignetted images have these SCTG properties.

2.2.1 Distribution Properties

Like the horizontal [21], vertical, and radial gradients [20], the semicircular tangential gradient distribution in a vignetting-free image is near-symmetric and heavy-tailed. The same is true of SCTGs for an image with vignetting when the estimated optical center is correct. However, when the estimated optical center is off from the true position in a vignetted image, SCTGs yield distributions that are asymmetric, as demonstrated in Fig. 2 and Fig. 3. The cause of this asymmetry is explained in Sec. 2.2.2, and the figures also show that distributions of conventional TGs and horizontal gradients do not have this property.

To emphasize asymmetries around the peaks of gradient distributions, we also display $\log(1 + |x|)$ histograms in Fig. 2 and Fig. 3, as was done in [20]. While the x -axis represents gradient values in a regular gradient distribution, the $\log(1 + |x|)$ histogram is constructed by re-scaling the x -axis of the regular distribution according to $\log(1 + |x|)$. Note that the negative (red) side of the histogram is folded

over to the positive (blue) side to facilitate comparison. In addition, the figures give a numerical measure of distribution asymmetry, which will later be defined in Sec. 3.

We have compared the numerical asymmetry values of over 65 natural vignetted images before and after vignetting correction. For each of the images, three estimates of the optical center were randomly chosen with a distance of 0, 10, and 20 pixels from the true optical center. The asymmetry values of the SCTG distributions were computed with each of the three hypothesized optical centers. Before vignetting correction, significant increases in asymmetry values were observed for greater distances from the true optical center, from an average of 0.05 for a correctly estimated center, to 0.14 for a 10-pixel error and 0.19 for a 20-pixel error. By contrast, after the vignetting correction no obvious changes were observed (0.054 *vs.* 0.051 *vs.* 0.057). That a greater estimation error generally corresponds to a higher asymmetry value in a vignetted image is a favorable property for optimization of the optical center, which is described in Sec. 3.

To compute an SCTG distribution and its asymmetry, the direction of the true optical center from the estimated optical center is needed, namely the angle θ_l in Eq. (6). To determine an approximate θ_l , we first obtain an initial value by sampling different angles $\theta_l = \{0, \frac{\pi}{10}, \frac{2\pi}{10}, \dots, \pi\}$ and taking the one that yields the greatest asymmetry, since asymmetry should generally be maximum for the correct value of θ_l . This and other asymmetry properties are examined in the following subsection. With this initialization, θ_l is then optimized as explained in Sec. 3.

2.2.2 Geometric Analysis

We now present a geometric analysis on the useful properties of SCTG distributions for optical center estimation. Since it is well known that the logarithms of image intensities have similar gradient distributions to that of the original image [21, 20], we examine images in the log domain for its convenience in analysis.

Let the vignetting-free image of Z be denoted by I , and the vignetting in Z by V , such that we have

$$Z(r', \theta') = I(r', \theta')V(r', \theta') \quad (7)$$

where (r', θ') are polar coordinates with the origin at the estimated optical center (x'_0, y'_0) . We also denote $\ln Z$, $\ln I$ and $\ln V$ by \mathcal{Z} , \mathcal{I} and \mathcal{V} , respectively, and represent the tangential gradients of \mathcal{Z} , \mathcal{I} and \mathcal{V} for each pixel (r', θ') by

$$\text{sgn}(x', y') = \begin{cases} 1, & \text{if } (0 \leq \theta_l < \pi) \& ((0 \leq \theta' \leq \theta_l) | (\theta_l + \pi \leq \theta' \leq 2\pi)) \\ 1, & \text{if } (\pi \leq \theta_l < 2\pi) \& (\theta_l - \pi \leq \theta' \leq \theta_l) \\ -1, & \text{else} \end{cases} \quad (6)$$

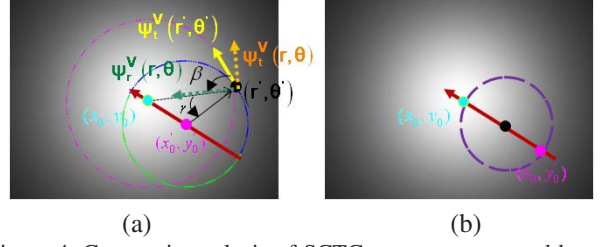


Figure 4. Geometric analysis of SCTG asymmetry caused by vignetting.

$\psi_t^{\mathcal{Z}}(r', \theta')$, $\psi_t^{\mathcal{I}}(r', \theta')$ and $\psi_t^{\mathcal{V}}(r', \theta')$. From Eq. 7, this gives us

$$\psi_t^{\mathcal{Z}}(r', \theta') = \psi_t^{\mathcal{I}}(r', \theta') + \psi_t^{\mathcal{V}}(r', \theta'). \quad (8)$$

On the RHS of Eq. (8), the first term is the TG of the vignetting-free image \mathcal{I} , which is assumed to have a symmetric distribution for natural images. The second term represents the TG for the vignetting component of the image, which is equal to zero when the estimated optical center lies at the true optical center. This leads to a symmetric SCTG distribution when the estimated optical center is correct. However, we will show that the second term is always non-negative for SCTGs when the estimated optical center is not correct, and this results in an asymmetric SCTG distribution.

Property 1: *The SCTG distribution is symmetric when the estimated optical center is at the true optical center, i.e., $(x'_0, y'_0) = (x_0, y_0)$.*

Since the estimated optical center is co-located with the true optical center, vignetting is radially symmetric about it. Because of this radial symmetry, the radial gradient of the vignetting component at a point (r', θ') with respect to the optical center (x'_0, y'_0) is equal to the gradient at that point [20]. Thus, the tangential gradient $\psi_t^{\mathcal{V}}(r', \theta')$ is zero, regardless of whether the SCTG is computed in the clockwise or counterclockwise direction. Since in Eq. (8) the distribution for the first term is symmetric and the second term is zero, the SCTG distribution is symmetric when the estimated optical center is correct.

Property 2: *The SCTG distribution is asymmetric when the estimated optical center is incorrect, i.e., $(x'_0, y'_0) \neq (x_0, y_0)$.*

When the estimated optical center is displaced from the true optical center, as shown in Fig. 4(a), the tangential gradient $\psi_t^{\mathcal{V}}(r', \theta')$ relative to the estimated optical center (x'_0, y'_0) is equal to the projection of the true radial gradient $\psi_r^{\mathcal{V}}(r, \theta)$ at that point onto the semicircular tangent direc-

tion, expressed as

$$\psi_t^y(r', \theta') = \psi_r^y(r, \theta) \cos(\beta) \quad (9)$$

where β is the rotation angle from $\psi_t^y(r', \theta')$ to $\psi_r^y(r, \theta)$.

From the property that vignetting is radially non-decreasing away from the true optical center, we show that SCTGs $\psi_t^y(r', \theta')$ are always non-negative. Let γ denote the rotation angle from $\psi_r^y(r, \theta)$ to the directional line from (r', θ') to (x'_0, y'_0) , as shown in Fig. 4(a). Since $\beta + \gamma = 90^\circ$, it can be seen by simple geometric reasoning on the triangle defined by (x_0, y_0) , (x'_0, y'_0) and (r', θ') that $0^\circ < \gamma < 180^\circ$ and $-90^\circ < \beta < 90^\circ$. This holds true both for pixels assigned clockwise or counterclockwise SCTG values. From Eq. (9) and the radially non-decreasing vignetting ($\psi_r^y(r, \theta) \geq 0$), we can conclude that $\psi_t^y(r', \theta') \geq 0$. Since the first term on the RHS of Eq. (8) has a symmetric distribution about zero and the second term skews the distribution towards positive values, the SCTG distribution is asymmetric about zero for vignetted images in which the estimated optical center is incorrect.

Property 3: *Asymmetry values of SCTG distributions generally increase with greater distances between the estimated and true optical centers.*

As seen in Fig. 4(a), for each pixel that does not lie on the line through (x'_0, y'_0) and (x_0, y_0) , β decreases for increasing distances between (x'_0, y'_0) and (x_0, y_0) . For pixels that lie within the circle defined by the diameter between (x'_0, y'_0) and (x_0, y_0) (shown in 4(b)), we have $90^\circ < \gamma < 180^\circ$ and a negative β . With negative values of β , the SCTG values for pixels within the circle become smaller (less positive) for increasing error in the estimated optical center. On the other hand, pixels outside the circle have $0^\circ < \gamma < 90^\circ$ and a positive β , which leads to larger (more positive) SCTG values. Consequently from Eq. (9), $\psi_t^y(r', \theta')$ becomes smaller for pixels inside the circle but larger for pixels outside the circle. Since there is typically a much larger number of pixels outside the circle than inside, the SCTG distribution will become more skewed in the positive direction when the distance between (x'_0, y'_0) and (x_0, y_0) becomes larger.

Property 4: *The asymmetry value for an SCTG distribution should generally be at its maximum for the correct value of θ_l in Eq. (6).*

For an estimated optical center, the angle θ_l defines the line that divides the assignment of pixels to clockwise or counterclockwise SCTGs, as illustrated in Fig. 1(b). As shown in the analysis of Property 2, SCTGs $\psi_t^y(r', \theta')$ are always non-negative given the true value of θ_l . An incorrect value of θ_l , however, leads to an erroneous line and wrong assignments of pixels to clockwise or counterclockwise SCTGs. A wrongly assigned pixel has an opposite sign for its SCTG, and therefore it will be non-positive. These

non-positive values decrease the positive skew of an SCTG distribution and reduce its asymmetry. Likewise, it can be seen that smaller errors in θ_l lead to fewer pixels with an incorrect SCTG sign, and thus greater asymmetry of the SCTG distribution. So the asymmetry value is generally maximized with the correct value of θ_l .

3. Optical Center Estimation from SCTG Distributions

With the properties of semicircular tangential gradient distributions described in Sec. 2, our algorithm estimates the optical center of an image with vignetting. Since an SCTG distribution is more symmetric with a more accurate estimate of θ_l and the optical center, our method seeks for the optical center (\hat{x}_0, \hat{y}_0) that minimizes asymmetry:

$$(\hat{x}_0, \hat{y}_0) = \arg \min_{(x'_0, y'_0)} \arg \max_{\theta_l} \Gamma(Z) \quad (10)$$

where $\Gamma(Z)$ represents the asymmetry of the SCTG distribution for an image Z .

Let $H(\psi_t^Z)$ denote the histogram of SCTGs in Z . Our asymmetry measure $\Gamma(Z)$ consists of two terms, the Kullback-Leibler (K-L) divergence $\mathcal{D}(H(\psi_t^Z))$ which describes the relative entropy between the positive and negative sides of the SCTG distribution, and the difference in histogram area between the negative (A_1) and positive (A_2) sides:

$$\Gamma(Z) = \lambda_h \mathcal{D}(H(\psi_t^Z)) + (1 - \lambda_h) |A_1 - A_2|^{\frac{1}{4}} \quad (11)$$

where λ_h is a weighting coefficient set empirically to 0.8 in our experiments, and the histogram areas are computed by

$$A_1 = \sum_{\psi_t^Z \leq 0} H(\psi_t^Z), \quad A_2 = \sum_{\psi_t^Z \geq 0} H(\psi_t^Z). \quad (12)$$

In evaluating $\mathcal{D}(H(\psi_t^Z))$, we take the negative and positive sides of the SCTG distribution $H(\psi_t^Z)$ as

$$H_-(\psi_t^Z) = \begin{cases} \frac{1}{A_1} H(-\psi_t^Z) & \psi_t^Z \geq 0 \\ 0 & \psi_t^Z < 0 \end{cases} \quad (13)$$

and

$$H_+(\psi_t^Z) = \begin{cases} \frac{1}{A_2} H(\psi_t^Z) & \psi_t^Z \geq 0 \\ 0 & \psi_t^Z < 0 \end{cases}. \quad (14)$$

Here, the sides of the histogram are mapped to probability distribution functions, and $\mathcal{D}(H(\psi_t^Z))$ measures the difference between the two probability distributions $H_+(\psi_t^Z)$ and $H_-(\psi_t^Z)$ in terms of the K-L divergence:

$$\mathcal{D}(H(\psi_t^Z)) = \sum_{\psi_t^Z} \left(H_+(\psi_t^Z) \cdot \log \frac{H_+(\psi_t^Z)}{H_-(\psi_t^Z)} \right). \quad (15)$$

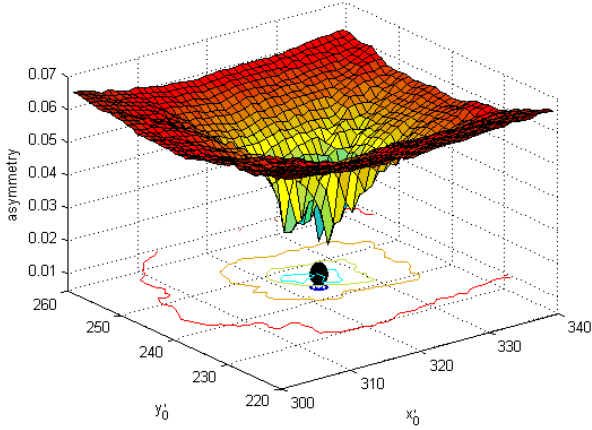


Figure 5. Profile of asymmetry measure with respect to different hypothesized positions of the optical center (x_0, y_0) for the image in Fig. 2. The true optical center is marked by the black circle.

Our method finds the optimal estimate of the optical center by minimizing the asymmetry of the SCTG distribution as in Eq. (10) using the Levenberg-Marquardt (L-M) algorithm [9]. We initialize (x'_0, y'_0) as the numerical center of the image coordinates, and θ_l as explained in Sec. 2.2.1. We repeat the two processes of estimating θ_l by fixing (x'_0, y'_0) and estimating (x'_0, y'_0) by fixing θ_l , until convergence. As shown in Fig. 5, the profile of the asymmetry measure with respect to the unknowns x'_0 and y'_0 enables quick convergence by L-M optimization to an accurate solution.

4. Results

We applied our algorithm to 480×640 images captured with a Canon G3, Canon EOS 20D, Nikon E775, and HP 945. For each camera, different focus and zoom settings were sampled to obtain various shifts of the camera’s optical center. Our algorithm was evaluated in three ways: estimation errors using images with simulated vignetting, errors using real images in comparison to ground truth, and improvements in single-image vignetting estimation [20] using our method as a preprocessing step.

4.1. Ground Truth Measurements

To obtain ground truth measurements of the optical center for each camera and setting, we use the DLR Camera Calibration Toolbox [12]. Ten images of a chessboard-like calibration panel were captured from different views and distances at each camera setting. The landmarks/corners of the panel were then detected with the DLR CalDe tool and some manual interaction. From the image coordinates of these calibration features, the intrinsic and extrinsic parameters of the camera were estimated with the DLR CalLab tool.

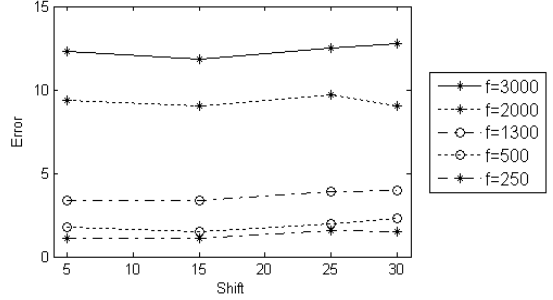


Figure 6. Errors in optical center estimation using images with simulated vignetting. The vignetting effects are simulated with different focal lengths f and random shifts of the optical center away from the numerical center of the image coordinates.

4.2. Experimental Evaluation

4.2.1 Simulated Data

We first simulated different vignetting effects using the off-axis illumination model in [4], which accounts for lens foreshortening as a function of focal length. In the simulation, we set $f = \{250, 500, 1300, 2000, 3000\}$ (in pixels) and added the simulated vignetting effects with optical centers randomized on circles centered at the numerical center of the image coordinates. These circles were sampled at four different radii (5, 15, 25 and 30 pixels), giving a total of 20 simulated vignetting effects. These effects were applied to a set of 65 real-world images considered to be vignetting-free, as they were captured with a large focal length. The simulated vignetting effects were added to each of the vignetting-free images by multiplying the original image intensities by the vignetting attenuation value. We show the estimation errors of our approach in Fig. 6, where the error value for each combination of f and optical center shift is averaged over the 65 images.

Since our algorithm relies on vignetting information to estimate the optical center, it becomes less effective for images captured with a larger focal length (weaker vignetting effects), as shown in Fig. 6. On the other hand, shifts in the optical center have little effect on the estimation accuracy of our approach.

4.2.2 Real Images

We also applied our algorithm to real images taken by the chosen cameras. The focal length and zoom were varied to obtain different optical centers [18], and we additionally varied the focus and aperture size to produce different vignetting characteristics. For each camera setting, we captured 15 images of real-world scenes. We ran our algorithm on each of these images, and present comparisons to ground truth values.

We found that the zoom parameter has little influence on

Zoom	z	27mm	40mm	90mm	136mm
Error	μ	1.0	1.3	1.1	1.0
	σ	0.6	1.9	0.7	0.7
Focal length	f	33mm	50mm	100mm	135mm
Error	μ	1.4	1.8	4.7	6.3
	σ	0.8	1.0	2.1	3.3
Focus	d	1m	5m	10m	∞
Error	μ	14.3	9.6	5.7	1.2
	σ	31.3	5.5	3.1	0.8
Aperture	a	f 5.6	f 4.5	f 3.5	f 2.8
Error	μ	14.1	13.3	8.4	1.5
	σ	21.0	18.9	7.8	0.9

Table 1. Error statistics (mean μ and standard deviation σ) with a Canon EOS 20D at different zooms z (with focal length 50mm), focal lengths f (27mm-136mm zoom), focus distances d (100mm zoom), and aperture sizes a (100mm zoom). Errors are measured in pixels.

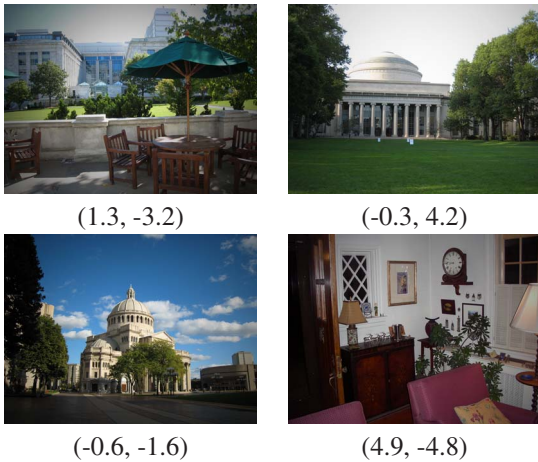


Figure 7. Estimation errors (in pixels) of our method for complex scenes.

our algorithm’s accuracy. By contrast, the focal length, the focus distance, and the aperture setting have more obvious effects, as shown in Table 1 which was computed from the 15 images. We only report the results for the Canon EOS 20D in Table 1. Results for the other cameras have very similar error statistics. We observe that camera settings that generate greater vignetting (shorter focal length, larger focus distance, and larger aperture size) usually lead to more accurate estimates of the optical center. With our technique, high accuracy can be obtained even for complex scenes such as those depicted in Fig. 7.

4.3. Application to Vignetting Correction

Finally, we applied our algorithm as a preprocess to the single-image vignetting correction algorithm of [20], which estimates and removes vignetting from a single input im-

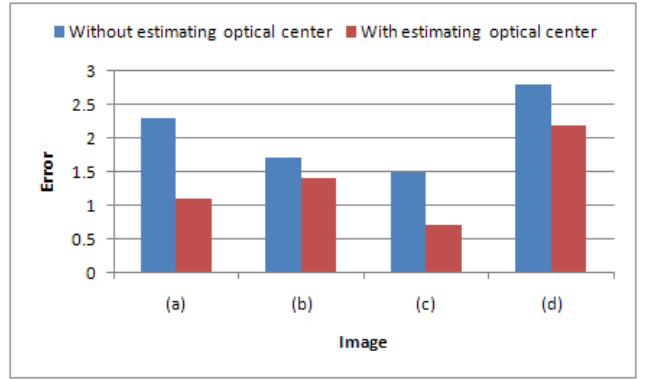


Figure 8. Mean Squared Errors ($\times 10^{-3}$) in the vignetting function estimated by the method in [20], with and without optical center estimation by our proposed method.

age of a real-world scene. The method in [20] assumes the optical center to be the numerical center of the image coordinates, but as this assumption does not always hold, errors in the optical center will inevitably lead to errors in the estimated vignetting function. In Fig. 8, we show the improvement in vignetting function estimation with the use of our method for optical center estimation. The ground truth vignetting effect was obtained using the method described in [19], and the errors were computed from sampled points on the vignetting function in the same manner as [19]. In this experiment, we used 20 real-world images captured from each of the four test cameras, with imaging parameters set to generate significant vignetting.

4.4. Speed

Our method performs optical center estimation in approximately 40 seconds for an image of size 480×640 . The algorithm was implemented in Matlab and run on a Dell PC with a 2.39 GHz Intel Core 2 CPU. A substantial increase in speed is likely to be possible with an optimized C++ implementation.

5. Conclusion

We have shown in this paper that it is possible to estimate the optical center given a single vignettted image of a natural scene. For this estimation, we introduced a new form of vignetting-based information called the semicircular tangential gradient. Through a geometric analysis, we showed that a correct estimate of the optical center results in a more symmetric SCTG distribution, and larger errors in the estimate leads to greater asymmetry in the distribution. From these properties, we proposed a technique to estimate the optical center by minimizing the asymmetry of the SCTG distribution.

The primary limitation of this approach is that vignetting must be present in the image. Our experiments have demon-

strated that greater levels of vignetting lead to higher estimation accuracy. Although this method lacks the overall accuracy of general camera calibration methods, it does not require special calibration targets or image sequences, which allows this technique to operate more broadly in scenarios where optical center estimation could not previously be performed, such as on downloaded web images. Moreover, the proposed method is highly useful for tasks such as vignetting correction [19, 20] which require an accurate estimation of the optical center.

Although we utilize the asymmetry measure proposed in our previous work [20], this paper and the work in [20] have fundamental differences. First, they solve two totally different tasks: correction of vignetting in [20] vs. estimation of optical center in our paper. Second, they use very differently defined gradients: radial gradient in [20] vs. SCTG in this paper. Third, optical center estimation in this paper can not only be used in improving the vignetting correction of [20] as shown in Sec. 4.3 but also in many other applications as explained in Sec. 1. Fourth, the optimization strategies are different as shown by Eq. (10) in our paper.

An interesting topic for future investigation is to extend our algorithm to perform optical center estimation from multiple images taken by a given camera with the same camera settings. Such a set of input images often exists in a photographer's collection. With this additional information, the accuracy of the optical center estimation may be appreciably improved.

ACKNOWLEDGEMENT

This publication was made possible by a grant from NSF Antarctic Sciences Division within the Office of Polar Programs (OPP0636726).

References

- [1] O. D. Faugeras and Q. t. Luong. Camera self-calibration: theory and experiments. In *ECCV*, pages 321–334, 1992.
- [2] R. Fergus, B. Singh, A. Hertzmann, S. T. Roweis, and W. T. Freeman. Removing camera shake from a single photograph. *ACM Transactions on Graphics*, 25(3):787–794, 2006.
- [3] R. I. Hartley, E. Hayman, L. D. Agapito, and I. Reid. Camera calibration and the search for infinity. In *ICCV*, pages 510–517, 1999.
- [4] S. Kang and R. Weiss. Can we calibrate a camera using an image of a flat textureless lambertian surface? In *ECCV*, volume II, pages 640–653, 2000.
- [5] R. K. Lenz and R. Y. Tsai. Techniques for calibration of the scale factor and image center for high accuracy 3-d machine vision metrology. *IEEE Trans. PAMI*, 10(15):713 – 720, 1988.
- [6] A. Levin and Y. Weiss. User assisted separation of reflections from a single image using a sparsity prior. In *ECCV*, 2004.
- [7] A. Levin, A. Zomet, and Y. Weiss. Learning how to inpaint from global image statistics. In *ICCV*, pages 305–312, 2003.
- [8] Y.-H. Lin and T. W. Low. Device and method for optical center detection. *US Patent Patent No.: US7,307,709 B2*, 2007.
- [9] W. H. Press, S. A. Teukolsky, W. T. Vetterling, and B. P. Flannery. *Numerical Recipes in C: The Art of Scientific Computing*. Cambridge University Press, New York, NY, USA, 1992.
- [10] S. Roth and M. J. Black. Steerable random fields. In *ICCV*, 2007.
- [11] G. Shivaram and G. Seetharaman. A new technique for finding the optical center of cameras. In *ICIP*, pages 167–171, 1998.
- [12] K. H. Strobl, W. Sepp, S. Fuchs, C. Paredes, and K. Arbter. DLR CalDe and DLR CalLab. In *Institute of Robotics and Mechatronics, German Aerospace Center (DLR)*.
- [13] M. Tappen, B. Russell, and W. Freeman. Exploiting the sparse derivative prior for super-resolution and image demosaicing. In *IEEE Workshop on Statistical and Computational Theories of Vision*, 2003.
- [14] R. Y. Tsai. A versatile camera calibration technique for high-accuracy 3d machine vision metrology using off-the-shelf tv cameras and lenses. *IEEE Journal of Robotics and Automation*, 3(4):323– 344, 1987.
- [15] L.-L. Wang and W.-H. Tsai. Computing camera parameters using vanishing-line information from a rectangular parallelepiped. *Machine Vision and Applications*, 3(3):129 – 141, 1990.
- [16] Y. Weiss and W. T. Freeman. What makes a good model of natural images? In *CVPR*, 2007.
- [17] R. G. Willson. *Modelling and calibration of automated zoom lenses*. PhD thesis, Carnegie Mellon University, Pittsburgh, PA., 1994.
- [18] R. G. Willson and S. A. Shafer. What is the center of the image? *Journal of the Optical Society of America A*, 11(11):2946 – 2955, 1994.
- [19] Y. Zheng, S. Lin, and S. B. Kang. Single-image vignetting correction. In *CVPR*, pages 461– 468, 2006.
- [20] Y. Zheng, J. Yu, S. B. Kang, S. Lin, and C. Kambhamettu. Single-image vignetting correction using radial gradient symmetry. In *CVPR*, 2008.
- [21] S. C. Zhu and D. Mumford. Prior learning and gibbs reaction-diffusion. *IEEE Trans. PAMI*, 19(11):1236– 1250, 1997.